Entanglement entropy in a time-dependent holographic Schwinger pair creation

Sebastian Grieninger,[1,*] Dmitri E. Kharzeev,[1,2,†] and Ismail Zahed[1,‡]

[1]*Center for Nuclear Theory, Department of Physics and Astronomy, Stony Brook University, Stony Brook, New York 11794–3800, USA*

[2]*Department of Physics, Brookhaven National Laboratory, Upton, New York 11973-5000, USA*

(Received 26 October 2023; accepted 29 November 2023; published 19 December 2023)

We analyze the entanglement of a Schwinger pair created by a time-dependent pulse. In the semiclassical approximation, the pair creation by a pulse of external electric field is captured by a periodic world line instanton. At strong gauge coupling, the gauge-gravity dual world sheet instanton exhibits a falling wormhole in AdS. We identify the tunneling time at the boundary with the inverse Unruh temperature, and derive the pertinent entanglement entropy between the created pair using thermodynamics. The entanglement entropy is enhanced by the subbarrier tunneling process, and partly depleted by the radiation in the postbarrier process.

DOI: 10.1103/PhysRevD.108.126014

I. INTRODUCTION

Schwinger pair creation [1] is a quantum process in which a pair of particles is produced from the vacuum in an external electric field. In quantum chromodynamics (QCD), the external chromoelectric field inside a confining string can lead to the production of a quark-antiquark pair, leading to string breaking when the string energy exceeds the light meson mass. This process is used in event generators (LUND, PYTHIA) [2] to account for jet fragmentation in high energy collisions [3].

The pair creation proceeds through tunneling, a quintessential quantum process. The vacuum pair tunnels through a potential barrier under the effect of a strong background field, and is produced with a finite probability. Throughout the creation process, the pair is correlated and interacts with both with the external (classical) field and the quantum gauge field. Quantum entanglement is the measure of these correlations throughout the pair history.

Recently, this pair creation process was used as an illustration of the Einstein-Rosen-Podolsky (EPR) paradox, in the context of quantum field theory at strong coupling [4,5]. In this strong coupling regime, the gravity dual of the pair is a string world sheet [6–15] with a nontraversable wormhole, or Einstein-Rosen (ER) bridge [4]. The quantum entanglement entropy of the pair is sensitive to the location of the ER bridge [4,16].

In the receding quark-antiquark pair in the Schwinger process, the endpoints of the string are never causally connected. However the pair is entangled owing to its color neutrality. In nonconfining dual gravity description, the entanglement entropy was found to be of order $\sqrt{\lambda}$ in the weak field limit [4,12,12,17,18], with $\lambda = g_Y^2 N_c$ the strong $'t$ Hooft coupling. In this work, we will extend our discussion which was restricted to static electric fields [17] and explore the entanglement in the pair creation process in the presence of a time-dependent electric pulse.

In QCD, a strong gauge field pulse could be generated by a highly boosted nucleus, assuming that all wee partons in the nuclear wave function add up coherently, see Refs. [19,20] and references therein. In the rest frame of a target interacting with this highly boosted nucleus, the target is crossed by a "gluon wall" [21] that is a pulse of gauge field. This pulse will lead to pair creation. The entanglement entropy of the pair can be converted to the Gibbs entropy of the final hadronic state. For QED, the equality between the entanglement and Gibbs entropies in Schwinger pair production by a pulse was demonstrated in [22]. For CFTs it was shown in [23] that the entanglement entropy across a spherical region is equal to the thermal entropy of the hyperbolic geometry $\mathbb{R} \times \mathbb{H}^{d-1}$, which is the direct product of time and the hyperbolic plane. In QCD, the effects of confinement have to be taken into account compared to the weak coupling QED calculation in [22], as well as radiation in the final state. Our present work addresses this problem from a holographic perspective.

*sebastian.grieninger@stonybrook.edu
†dmitri.kharzeev@stonybrook.edu
‡ismail.zahed@stonybrook.edu

The organization of the paper is as follows: In section II we briefly review the semiclassical analysis of the Schwinger process for particle pair creation by a pulse. The world line instanton solution is discussed, and an estimate of its entanglement entropy is given. In Sec. III, we extend the analysis to strong coupling, where the dual of the world line is a world sheet in AdS. The world sheet is characterized by a moving wormhole, a hallmark of the time-varying pulse at the boundary. We show that the entanglement entropy receives a positive contribution from tunneling (subbarrier process) and a negative contribution from radiation loss (postbarrier process). Our conclusions are in Sec. V.

II. TUNNELING IN A TIME-DEPENDENT EXTERNAL FIELD

Consider first a scalar particle of mass M, in an Abelianized external field moving in proper time, with the action

$$S = \int d\tau M\sqrt{\dot{x}^2} + i\oint A \tag{1}$$

Tunneling in (1) is captured by the world line instanton solution to the classical equations of motion in Euclidean signature,

$$M\frac{d}{d\tau}\left(\frac{\dot{x}_\mu}{\sqrt{\dot{x}^2}}\right) = iF_{\mu\nu}\dot{x}_\nu. \tag{2}$$

For a time dependent pulse electric field in Minkowski signature,

$$E(t) = \frac{E}{\cosh^2(\omega t)} \tag{3}$$

the Euclideanized vector potential in (1)

$$A_3(x_4) = \frac{-iE}{\omega}\tan(\omega x_4) \tag{4}$$

is purely imaginary. Since (4) is singular for $x_{4S} = \frac{\pi}{2\omega}$, all world lines are bounded by this maximum value in $|x_4| \leq x_{4S}$.

A. World line instanton

The tunneling process was discussed by many [24–31], with the instanton solution given by [27]

$$x_3(\tau) = \frac{1}{a\gamma}\frac{1}{\sqrt{1+\gamma^2}}\text{arcsinh}\left(\gamma\cos\left(a\sqrt{1+\gamma^2}\tau\right)\right) \equiv \frac{1}{a\bar{\gamma}}\sinh^{-1}(\gamma\cos(\bar{a}\tau))$$
$$x_4(\tau) = \frac{1}{a\gamma}\arcsin\left(\frac{\gamma}{\sqrt{1+\gamma^2}}\sin\left(a\sqrt{1+\gamma^2}\tau\right)\right) \equiv \frac{1}{a\gamma}\sin^{-1}(\underline{\gamma}\sin(\bar{a}\tau)). \tag{5}$$

It is periodic, with period

$$\beta = \frac{2\pi}{\bar{a}} \equiv \frac{2\pi}{a\sqrt{1+\gamma^2}} \tag{6}$$

with $a = E/M$ and $\gamma = \omega/a$.

Throughout, $E \equiv g_Y E$ refers to the invariant electric field in the probe D3 brane. Eqs. (5) describe a cyclotron-like trajectory that satisfies $\dot{x}_3^2 + \dot{x}_4^2 = 1$, since the applied force in (2) is magnetic in Euclidean signature. The Wilson loop traced by the boundary world line (5) is ellipticlike in general,

$$\frac{\text{sh}^2(a\bar{\gamma}x_3)}{\gamma^2} + \frac{\sin^2(a\gamma x_4)}{\underline{\gamma}^2} = 1 \tag{7}$$

as illustrated in Fig. 1. The high eccentricity of the trajectories along the x_4 direction follows from the singularity of the force from the pulse, at $x_{4S} = \frac{\pi}{2\omega}$ of (1) noted

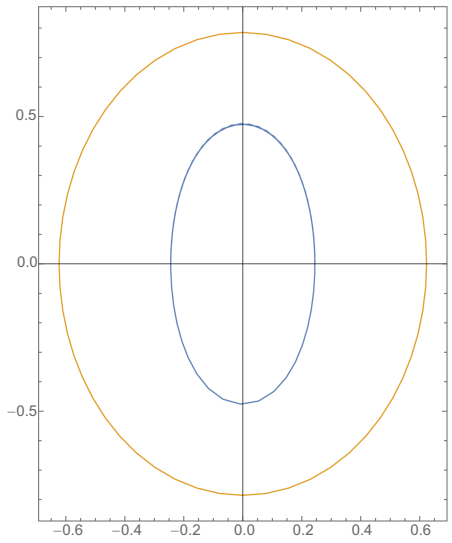

FIG. 1. Contour plot of (7) for $a = \gamma = 1$ (outer) and $a = 1$, $\gamma = 2.5$ (inner) with $M = 1$.

earlier. It becomes circular in the static limit, $x_3^2 + x_4^2 \to \frac{1}{a^2}$ as $\omega \to 0$.

B. Particle entanglement

For scalar pair creation of mass $2M$, the action evaluated using (5) is

$$S(\beta) = \frac{\beta M}{1 + (1 - (\beta\omega/2\pi)^2)^{\frac{1}{2}}} \tag{8}$$

with $e^{-2S(\beta)}$, the penalty for tunneling in the absence of confinement. When the pulse is about static, $S(\beta) \sim \frac{1}{2}\beta M$ in agreement with Schwinger's original result. Alternatively, when the pulse is very sharp in time, $S(\beta) \sim \frac{2\pi M}{\omega}$. At large frequency, the pair production is uninhibited.

We interpret (8) as the free energy $S(\beta) = \beta F(\beta)$ of the tunneling pair in the pulse. As a result, the corresponding quantum entropy at the boundary, is given by thermodynamics

$$S^B_{EE} = \frac{\beta M \gamma^2}{(1 + \sqrt{1+\gamma^2})^2} \tag{9}$$

It vanishes in the static limit as $S^B_{EE} \sim \beta M \gamma^2$, and for large frequencies vanishes as $S^B_{EE} \sim \frac{2\pi M}{\omega}$.

III. HOLOGRAPHIC PAIR PRODUCTION

The world line instanton (5) captures the pair production of a particle of mass M at the boundary, at weak coupling. In the double limit of strong 't Hooft coupling λ and large N_c, the gravity dual description is captured by a string world sheet sourced by the boundary Wilson loop on a D3 brane. Holographic pair production of particles as end points of strings, extends (1) to the Nambu-Goto action in bulk

$$S = \sigma_T \int \mathrm{d}\tau \mathrm{d}\sigma |\det g_{MN} \partial_\tau X^M \partial_\sigma X^N|^{\frac{1}{2}} + i \oint A \tag{10}$$

in AdS_5 with line element

$$\mathrm{d}s^2 = g_{MN}\mathrm{d}x^M \mathrm{d}x^N = \frac{L^2}{z^2}(\mathrm{d}x_\mu^2 + \mathrm{d}z^2) \tag{11}$$

with $\sigma_T L^2 = \sqrt{\lambda}/2\pi$. The coordinate embedding of the string $X^M(\tau, \sigma)$ can be obtained numerically in Euclidean signature, using the Nambu-Goto action for the string in bulk, as constrained by the Wilson loop at the D3 boundary.

A. Euclidean string world sheet

In Euclidean signature, the world sheet surface in bulk is ellipsoidal. To parametrize it in AdS_5, we use cylindrical coordinates r, φ, z,

$$x^M(z, \varphi) = (0, 0, r(z,\varphi)\cos(\varphi), r(z,\varphi)\sin(\varphi), z) \tag{12}$$

in terms of which the Nambu-Goto action plus the electric field at the boundary, read

$$S = \frac{\sqrt{\lambda}}{2\pi}\int_{z_M}^{z_E} \mathrm{d}z \int_0^{2\pi} \mathrm{d}\varphi \frac{1}{z^2}(r^2(1 + r_z^2) + r_\varphi^2)^{\frac{1}{2}} + i \oint A \tag{13}$$

with the shorthand notation $r_z = \partial_z r$ and $r_\varphi = \partial_\varphi r$. Here z_M is the position of the probe D3 brane, with $z_M = \frac{\sqrt{\lambda}}{2\pi M}$ fixed by the mass of the probe D3 brane at the boundary. Here z_E is the tip (extrema) of the ellipsoidal-like world sheet in bulk,

$$r(z_E, \varphi) = 0 \qquad r_z(z_E, \varphi) = \infty \tag{14}$$

In (13) we have used the fact that the electric field (5) acts as a magnetic field in Euclidean signature, with the "vector potential" (4). Its contribution to the Wilson loop at the boundary $z = z_M$, is

$$i \oint A = \int_0^{2\pi} \mathrm{d}\varphi \frac{E}{\omega} \tan(\omega r \sin\varphi)(\cos\varphi r_\varphi - r\sin\varphi) \tag{15}$$

The bulk equation of motion follows by variation

$$-r r_{zz}(r^2 + r_\varphi^2) + r r_{\varphi\varphi}(1 + r_z^2) - \frac{2}{z} r_\varphi (r^2(1 + r_z^2) + r_\varphi^2) - r^2 r_z^2 - 2r_\varphi^2 - 2r r_z r_\varphi r_{z\varphi} - r^2 = 0 \tag{16}$$

subject to the Lorentz force along the z-direction at the D3 brane on the boundary at $z = z_M$,

$$\frac{\sqrt{\lambda}}{2\pi}\frac{1}{z_M^2}\frac{r^2 r_z}{(r^2(1+r_z^2)+r_\varphi^2)^{\frac{1}{2}}} = \frac{E}{\cos^2(\omega r \sin\varphi)}\left(r - \frac{1}{2} r_\varphi \sin 2\varphi\right). \tag{17}$$

Again, we made use of the short hand notations $r_{zz} = \partial_z^2 r$, $r_{\varphi\varphi} = \partial_\varphi^2 r$, and $r_{z\varphi} = \partial_z \partial_\varphi r$. (16) subject to the boundary condition (17) can be solved numerically using the pseudo-spectral methods (with Chebychev discretization in the radial direction and Fourier discretization in φ).

In Fig. 2 (left) we show the Euclidean surface for $z_M E = 0.44$ and $z_M \omega = 0.25$. The on-shell action S_{OS} of the ellipsoidal surface (13), sets the tunneling probability for the holographic pair production in the pulse, in the strong field limit. In Fig. 3 (left) we show the behavior of the on-shell action versus $T = 1/\beta$ given in (6), for increasing

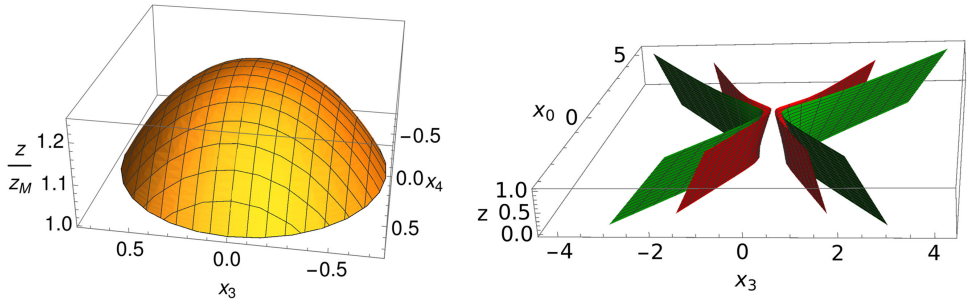

FIG. 2. Left: Subbarrier Euclidean string world sheet, for pair production in a pulse for $z_M E = 0.44$ and $z_M \omega = 0.25$. Right: Postbarrier Minkowski string world sheet, for pair production in a pulse, for $\gamma = a = 1$ (green) and $\gamma = 2$, $a = 1$ (red), with $z_M = 0$.

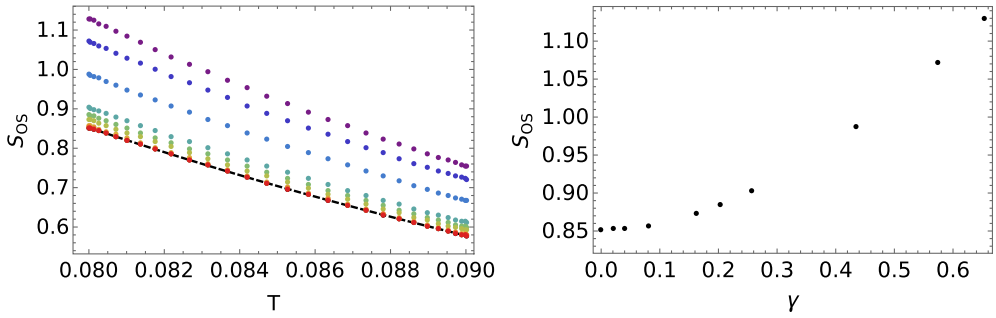

FIG. 3. Left: On-shell action vs $T = 1/\beta$ for different ω (increasing from red to purple). The analytical result for $\omega = 0$ is the black dashed line. Right: On-shell action vs γ for $T = 0.08$ and $\lambda = 12$.

frequencies of the pulse from bottom-red to top-purple. The numerical results shown in the dashed-black curve for $\omega = 0$, coincide with the analytical results for the holographic pair production derived in [8]

$$S_{OS} \to \frac{\sqrt{\lambda}}{2}\left(\sqrt{\frac{T_c}{T}} - \sqrt{\frac{T}{T_c}}\right)^2 \tag{18}$$

with

$$T_c = \frac{a_c}{2\pi} = \frac{1}{2\pi}\frac{1}{\sqrt{R^2 + z_M^2}}.$$

Our numerical results, generalize (28) to a time-dependent pulse.

In Fig. 3 (right) we show the on-shell action versus $\gamma = M\omega/E$ for fixed temperature. The increasing action reflects on the larger penalty for the pair production rate, with larger ω and fixed E as the pulse is short lived. Equivalently, the larger E for fixed ω, the smaller the penalty for pair production.

B. Particle multiplicities in a pulse

Strong and coherent chromoelectric pulses can be produced during the initial phase of an ultrarelativistic heavy-ion collision. The higher the energy of the ion projectile, the stronger the field and the shorter is its duration in the frame of the target.

Strong chromoelectric fields can produce light quark pairs through the Schwinger mechanism. For the strongly coupled phase, the mean number of produced pairs in the pulse is

$$\bar{n} = \sum_{n=1}^{\infty} n p_n = \sum_{n=1}^{\infty} n(e^{S_{OS}} - 1)e^{-nS_{OS}} = \frac{1}{1 - e^{-S_{OS}}}$$

In Fig. 4, we show the dependence of the mean number of produced particles on $\gamma = M\frac{\omega}{E}$ (not to be confused with the Lorentz contraction factor). The mean number of produced pairs decreases with increasing γ, since tunneling is more

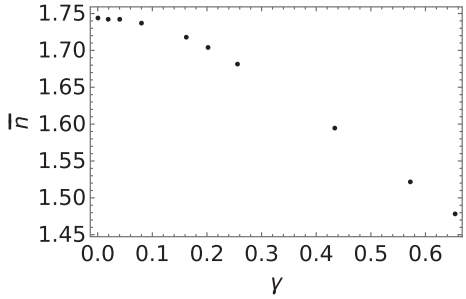

FIG. 4. Mean number of particles produced in the pulse as a function of $\gamma = M\frac{\omega}{E}$ for $T = 0.08$, $z_M = 1$ and $\lambda = 12$.

suppressed (note that the case of strong and static electric fields corresponds to $\gamma \to 0$.)

C. Minkowski string world sheet

In Minkowski signature, the world sheet in bulk is the locus of the retarded radiation, sourced by an accelerating $q\bar{q}$ pair tracing the Wilson loop with hyperboliclike world lines. It follows from the ruled surface in bulk [32]

$$X^M(t,z) = (z\dot{x}^\mu(t) + x^\mu(t), z) \tag{19}$$

with $\sigma = z$. The boundary world lines

$$x^\mu(t) = (x^0(t), 0, 0, x^3(t))$$

follow from (5) by analytical continuation $\tau \to it$ and $ix_4 \to x_0$,

$$\begin{aligned} x^3(t) &= \frac{1}{a\bar{\gamma}} \sinh^{-1}(\gamma \cosh(\bar{a}t)) \\ x^0(t) &= \frac{1}{a\gamma} \sinh^{-1}(\underline{\gamma} \sinh(\bar{a}t)) \end{aligned} \tag{20}$$

with $\dot{x}_\mu^2 = -1$. In Fig. 2 (right) we show two world sheets as given by (19) and traced by (20) with $\gamma = a = 1$ (green) and $\gamma = 2$, $a = 1$ (red). We have set $z_M = 0$ for the D3 brane for convenience. For $\gamma = 0$, the ruled surface (right) is the analytical continuation of the Euclidean surface (left), as initially observed in [4,5].

D. Moving wormhole on the world sheet

The time-dependent string world sheet harbors a moving wormhole. To see this, consider the line element associated to (19)

$$\mathrm{d}X_M^2 = \left(a^2(t) - \frac{1}{z^2}\right)\mathrm{d}t^2 - \frac{2}{z^2}\mathrm{d}t\mathrm{d}z \tag{21}$$

with a squared acceleration

$$a^2(t) \equiv \ddot{x}^2 = a^2(1 + \underline{\gamma}^2 \sinh^2(\bar{a}t))^{-2} \tag{22}$$

and an effective horizon at $z_H(t) = 1/a(t)$. In the static limit $\omega \to 0$, it reduces to the static horizon $z_H \to \frac{1}{a}$. Away from the static limit, the horizon is moving away from the boundary, with asymptotically

$$z_H(t) \sim \frac{\gamma\underline{\gamma}}{4\bar{a}} e^{2\bar{a}t} \tag{23}$$

The black hole is falling rapidly in bulk, a hallmark of a time-dependent problem [33–35].

IV. ENTANGLEMENT FOR THE PULSING STRING

The effective horizon $z_H(t)$ splits the world sheet in bulk into a causal part with $z < z_H(t)$ and a noncausal part with $z > z_H(t)$. This is also the location of a time-dependent wormhole, as observed in [4] for the static case.

The entanglement entropy (EE) receives contribution from both the causal part of the world sheet (positive) and noncausal part of the world sheet (negative). We will distinguish between the weak field limit and strong coupling where the world sheet surface can be obtained both analytically and numerically (for the causal part only), and the strong field and strong coupling limit where the world sheet surface can only be obtained numerically.

A. Causal contribution to EE: Weak field limit

The causal contribution to the entanglement entropy in the weak field limit and finite $\gamma = M\omega/E$ is given numerically by the Euclidean surface, and more explicitly by the ruled surface in Minkowski signature, as we have discussed in [17]. Specifically, the causal contribution of the world sheet action

$$\begin{aligned} S^C &= 2 \times \frac{\sqrt{\lambda}}{2\pi} \int_{-\frac{1}{2}\mathcal{T}}^{+\frac{1}{2}\mathcal{T}} \mathrm{d}t \int_{z_M}^{\frac{1}{a(t)}} \frac{\mathrm{d}z}{z^2} \\ &= 2 \times \frac{\sqrt{\lambda}}{2\pi} \int_{-\frac{1}{2}\mathcal{T}}^{+\frac{1}{2}\mathcal{T}} \mathrm{d}t \left(\frac{1}{z_M} - a(t)\right) \end{aligned} \tag{24}$$

The first contribution [from the minuend in (24)] reduces to the rest mass contribution

$$S^C_{(1)} = \frac{\sqrt{\lambda}}{\pi z_M} \int_{-\frac{1}{2}\mathcal{T}}^{+\frac{1}{2}\mathcal{T}} \mathrm{d}t = 2 \times \mathcal{T} \frac{\sqrt{\lambda}}{2\pi z_M} = 2\mathcal{T}M. \tag{25}$$

For $\omega \neq 0$, the time integration of the subtracted term in (24) gives

$$\begin{aligned} S^C_{(2)} &= -\frac{\sqrt{\lambda}}{\pi} \int_{-\frac{1}{2}\mathcal{T}}^{+\frac{1}{2}\mathcal{T}} \mathrm{d}t a(t) \\ &= 2 \times \frac{\sqrt{\lambda}}{2\pi} \ln \left| \frac{(\sqrt{1+\gamma^2}+1)e^{-\bar{a}\mathcal{T}} + \sqrt{1+\gamma^2} - 1}{(\sqrt{1+\gamma^2}-1)e^{-\bar{a}\mathcal{T}} + \sqrt{1+\gamma^2} + 1} \right| \end{aligned} \tag{26}$$

after using (22).

In the large $\mathcal{T}$ limit, (26) reduces to

$$S^C_{(2)}(\mathcal{T} \to \infty) = 2 \times \frac{\sqrt{\lambda}}{2\pi} \ln \left| \frac{\sqrt{1+\gamma^2} - 1}{\sqrt{1+\gamma^2} + 1} \right|. \tag{27}$$

In the small frequency limit with $|\gamma| \ll 1$, (27) reduces to $-\frac{2\sqrt{\lambda}}{\pi} \ln |\frac{1}{\gamma}|$, which is to be compared to [17]

$$2M\mathcal{T} - 2\sqrt{\lambda}\mathcal{T}/\beta \tag{28}$$

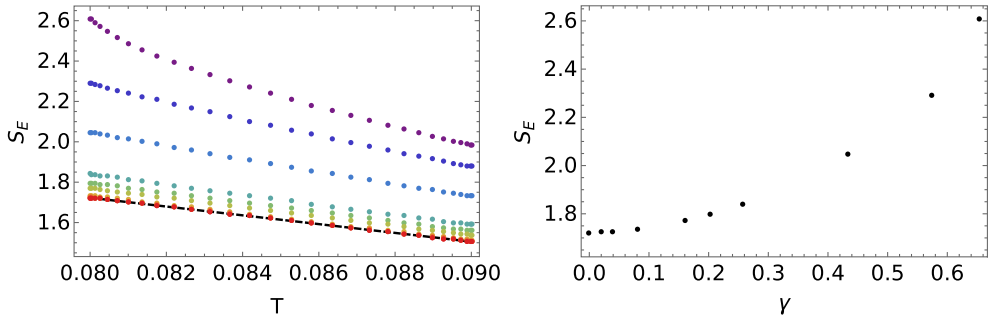

FIG. 5. Left: entanglement entropy as a function of the temperature $T = 1/\beta$ for different ω (increasing from red to purple). The analytical result for $\omega = 0$ is the black dashed line. Right: entanglement entropy as a function of $\gamma = \omega/a$ for $T = 0.08$, $z_M = 1$ and $\lambda = 12$.

in the static limit. This limit is singular and does not reduce to our static result [17]. We conclude that the small frequency limit does not commute with the large time limit. If we take the small frequency limit first, then (26) reduces to

$$S^C_{(2)}(\omega \to 0) = -2\sqrt{\lambda}T\mathcal{T} + \sqrt{\lambda}\frac{\sinh(2\pi T\mathcal{T})}{8\pi^3 T}\omega^2 + O(\omega^4). \tag{29}$$

Equation (29) correctly reproduces the static case considered in [17]. In the following, we assume that ω is sufficiently large. Recall, that we are in the weak field limit, i.e. $E = M \cdot a \ll 1$. In the weak field limit, (26) reduces to

$$S^C_{(2)}(a \to 0) = -\frac{2\sqrt{\lambda}\sqrt{4\pi^2T^2 - \omega^2}\tanh(\frac{\mathcal{T}\omega}{2})}{\pi\omega} + O(a^3). \tag{30}$$

If ω is not too small, we can safely take the large $\mathcal{T}$ limit with $\tanh(\mathcal{T}\omega/2) \to 1$. Hence, $S^C_{(2)}$ is finite in the large $\mathcal{T}$ limit and thus subleading.

With this in mind and using (28), the causal contribution is

$$S^C = 2\mathcal{T}M - 2\sqrt{\lambda}\mathcal{T}/\beta(1 - \theta(|\gamma|)) + \mathcal{O}(\mathcal{T}^0) \tag{31}$$

This is expected for $\gamma \neq 0$, since the effective horizon asymptotes the Poincaré singularity for large times as we noted in (23). At late times, the self-energy is solely due to the mass following from the D3 brane, with no Debye screening mass induced by the rapid fall off. We now interpret the causal part of the action $F^C = S^C/\beta$ as a *free energy* for fixed temperature $T = 1/\beta$ [17]. In the weak field limit, the causal contribution of the EE for the pulse is then identified through thermodynamics

$$S^C_{EE}(\gamma) = \beta^2\frac{\partial F^C}{\partial\beta} = \sqrt{\lambda}(1 - \theta(|\gamma|)) + \mathcal{O}(\mathcal{T}^0), \tag{32}$$

which is equal to zero at late times for finite $|\gamma|$.

B. Causal contribution to EE: Strong field limit

The causal contribution to the entanglement entropy in the strong field limit, is solely given by the numerically generated Euclidean world sheet, using the arguments we presented in [17]. Again, we can regard the on-shell action $S_{OS} = \beta F_{OS}$ as a function of the temperature $T = 1/\beta$ shown in Fig. 3 (left), as a *free energy* F_{OS}. In the strong field limit, the EE is again identified through thermodynamics

$$S^C_E = \beta^2\frac{\partial F_{OS}}{\partial\beta}. \tag{33}$$

In Fig. 5 (left) we show the numerical results for the EE as given by (33) versus temperature $T = 1/\beta$, for different pulse frequencies ω. The curves are for increasing frequencies from bottom-red to top-purple. The black-dashed curve is the exact result [17] for $\omega = 0$.

In the right side of Fig. 5, we show the EE versus $\gamma = \omega/a$. In the pulsing electric field, the EE is continuously enhanced.

C. Noncausal contribution to EE: Weak field limit

The noncausal part of the entanglement entropy, amounts to evaluating the radiation loss across the falling horizon. This is readily done by noting that (19) with the time-dependent acceleration (22), captures the Larmor radiation at strong coupling [32]

$$\mathcal{E}_R = \frac{\sqrt{\lambda}}{2\pi}\int_{-\frac{1}{2}\mathcal{T}}^{+\frac{1}{2}\mathcal{T}} dt a^2(t) = \frac{a\sqrt{\lambda}}{4\pi}\left(-(2+\gamma^2)\ln\left|\frac{(\sqrt{1+\gamma^2}+1)e^{-\bar{a}\mathcal{T}} + \sqrt{1+\gamma^2} - 1}{(\sqrt{1+\gamma^2}-1)e^{-\bar{a}\mathcal{T}} + \sqrt{1+\gamma^2} + 1}\right| - \frac{\gamma^2\sqrt{1+\gamma^2}(e^{\bar{a}\mathcal{T}} - e^{-\bar{a}\mathcal{T}})}{\frac{\gamma^2}{2}(e^{-\bar{a}\mathcal{T}} + e^{\bar{a}\mathcal{T}}) + \gamma^2 + 2}\right) \tag{34}$$

which simplifies in the large time limit to

$$-\frac{a\sqrt{\lambda}}{4\pi}\left(2\sqrt{\gamma^2+1}+(\gamma^2+2)\ln\left|\frac{\sqrt{1+\gamma^2}-1}{\sqrt{1+\gamma^2}+1}\right|\right).$$

The radiation loss of the entanglement entropy follows by interpreting (34) as free energy and taking the derivative with respect to the temperature. The temperature follows by using (6) to redefine the acceleration in terms of the effective temperature for fixed ω as in (6). If we identify $\mathcal{T}=N/T$ as the luminal time it takes the radiation to fall to the effective horizon [17], the entanglement entropy follows as $S_{EE}^{NC}=-\partial\mathcal{E}_R/\partial T$. The constant $\mathcal{N}$ fixes the time it takes to reach the horizon and was determined in [17,32] as $\mathcal{N}=1/(3\pi)$. Hence, we find

$$\frac{S_{EE}^{NC}(\gamma)}{\sqrt{\lambda}}=-\frac{1}{2}\sqrt{1+\gamma^2}\left(\frac{2\sqrt{1+\gamma^2}\gamma^2(e^{4/3}-1)((1+e^{2/3})^2\gamma^2+12e^{2/3})}{((1+e^{2/3})^2\gamma^2+4e^{2/3})^2}+(\gamma^2-2)\log\left(\frac{\sqrt{1+\gamma^2}-\tanh(\frac{1}{3})}{\sqrt{1+\gamma^2}+\tanh(\frac{1}{3})}\right)\right) \tag{35}$$

where e is Euler's number.

A few comments are in order. Unlike in the last subsection, we did not have to take a large $\mathcal{T}$ limit since it takes only a finite amount of time to reach the world sheet horizon. In fact, setting γ to zero reduces the EE to $S_{EE}^{NC}(0)=-\frac{2}{3}\sqrt{\lambda}$ as we observed in the static case in [17]. Moreover, the expression (35) is in general negative, or a loss due to radiation.

D. Estimate of net EE: Strong field

The net EE in the pulse, is the sum of the causal contribution due to tunneling (positive) and the noncausal contribution due to radiation (negative). In the strong field limit, the former follows from the Euclidean surface using (33) as shown in Fig. 5 (left). In contrast, the radiation part following from the ruled world-sheet surface, only accounts for the radiation in the weak-field limit (no backreaction) as we argued in [17]. To remedy for this, we suggest an estimate for the net EE as

$$S_{EE}=S_{EE}^{C}+\left(S_{EE}^{NC}+\sqrt{\lambda}\frac{T}{T_c}\right) \tag{36}$$

Note that with the added extra contribution, it reduces to the strong field limit discussed in [17] for $\omega=0$. As shown in Fig. 6, the radiation loss in Eq. (36) slightly overpowers the gain in the causal entanglement entropy for intermediate $\gamma=M\omega/E$, before being overtaken by the latter for larger γ. The dots in Fig. 6 are the numerical result for (36) with S_{EE}^{C} following numerically from (33), and S_{EE}^{NC} given by (35) corrected by $\frac{2}{3}$.

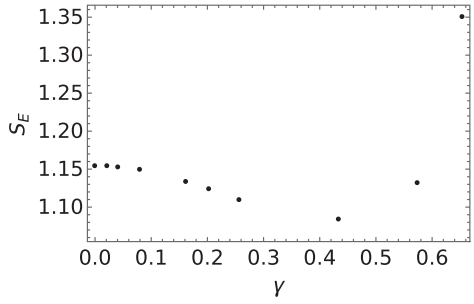

FIG. 6. Net entanglement entropy for pair production in a pulse as in (36) for $T=0.08$, $z_M=1$ and $\lambda=12$.

The dots are the numerical results for (36) with S_{EE}^{C} following numerically from (33), and S_{EE}^{NC} given by (35).

V. CONCLUSIONS

In the semiclassical approximation at weak coupling, the Schwinger pair creation by an electric pulse is captured by a periodic world line instanton. The inverse period of the instanton can be identified with the Unruh temperature.

The pair production in an electric pulse at strong coupling in the gravity dual description is described by a world sheet instanton. We have found the corresponding world sheet in Minkowski signature in the weak field limit. In the strong field limit, we have obtained numerically the tunneling surface, thereby generalizing the holographic Schwinger pair production process in a constant electric field [8] to time-dependent electric pulses.

Remarkably, the gravity dual string world sheet exhibits a falling wormhole that acts as a separatrix splitting the world sheet into a causal and acausal part which is hidden behind the horizon. In the weak field limit and under the assumption that ω is sufficiently large, the causal part of the world sheet does not generate any entanglement entropy to leading order at late times, and all of it results from the radiation in the acausal part.

This is not the case in the strong field limit, where the causal part of the world sheet can be captured by the Euclidean surface. Indeed, the numerically generated Euclidean world sheet results in a positive contribution to the entanglement entropy.

It would be interesting to derive the strong field expression for the contribution to the entanglement entropy from radiation. Moreover, in the weak field limit, it would be illuminating to work out the subleading contributions to the causal part of the entanglement entropy and see if it yields a net positive entanglement entropy at intermediate times.

ACKNOWLEDGMENTS

This work was supported by the U.S. Department of Energy, Office of Science, Office of Nuclear Physics, Grants No. DE-FG88ER41450 and No. DE-SC0012704 (DK), and the U.S. Department of Energy, Office of Science, National Quantum Information Science Research Centers, Co-design Center for Quantum Advantage (C2QA) under Contract No. DE-SC0012704 (DK).

[1] Julian S. Schwinger, On gauge invariance and vacuum polarization, Phys. Rev. **82**, 664 (1951).
[2] Bo Andersson, G. Gustafson, G. Ingelman, and T. Sjostrand, Parton fragmentation and string dynamics, Phys. Rep. **97**, 31 (1983).
[3] D. Buskulic *et al.* (ALEPH Collaboration), Measurements of the charged particle multiplicity distribution in restricted rapidity intervals, Z. Phys. C **69**, 15 (1995).
[4] Kristan Jensen and Andreas Karch, Holographic dual of an Einstein-Podolsky-Rosen pair has a wormhole, Phys. Rev. Lett. **111**, 211602 (2013).
[5] Julian Sonner, Holographic Schwinger effect and the geometry of entanglement, Phys. Rev. Lett. **111**, 211603 (2013).
[6] A. S. Gorsky, K. A. Saraikin, and K. G. Selivanov, Schwinger type processes via branes and their gravity duals, Nucl. Phys. **B628**, 270 (2002).
[7] Bo-Wen Xiao, On the exact solution of the accelerating string in AdS(5) space, Phys. Lett. B **665**, 173 (2008).
[8] Gordon W. Semenoff and Konstantin Zarembo, Holographic Schwinger effect, Phys. Rev. Lett. **107**, 171601 (2011).
[9] Aitor Lewkowycz and Juan Maldacena, Exact results for the entanglement entropy and the energy radiated by a quark, J. High Energy Phys. 05 (2014) 025.
[10] Mariano Chernicoff, Alberto Güijosa, and Juan F. Pedraza, Holographic EPR pairs, wormholes and radiation, J. High Energy Phys. 10 (2013) 211.
[11] Kristan Jensen, Andreas Karch, and Brandon Robinson, Holographic dual of a Hawking pair has a wormhole, Phys. Rev. D **90**, 064019 (2014).
[12] Veronika E. Hubeny and Gordon W. Semenoff, Holographic accelerated heavy quark-anti-quark pair, arXiv: 1410.1172.
[13] Mahdis Ghodrati, Schwinger effect and entanglement entropy in confining geometries, Phys. Rev. D **92**, 065015 (2015).
[14] Gordon W. Semenoff, Lectures on the holographic duality of gauge fields and strings, *Integrability: From Statistical Systems to Gauge Theory* (Oxford University Press, New York, 2019).
[15] Chen-Pin Yeh, Shock waves in holographic EPR pair, arXiv:2310.00991.
[16] Juan Maldacena and Leonard Susskind, Cool horizons for entangled black holes, Fortschr. Phys. **61**, 781 (2013).
[17] Sebastian Grieninger, Dmitri E. Kharzeev, and Ismail Zahed, Entanglement in a holographic Schwinger pair with confinement, Phys. Rev. D **108**, 086030 (2023).
[18] Veronika E. Hubeny and Gordon W. Semenoff, String worldsheet for accelerating quark, J. High Energy Phys. 10 (2015) 071.
[19] Francois Gelis, Edmond Iancu, Jamal Jalilian-Marian, and Raju Venugopalan, The color glass condensate, Annu. Rev. Nucl. Part. Sci. **60**, 463 (2010).
[20] Yuri V. Kovchegov and Eugene Levin, *Quantum Chromodynamics at High Energy* (Oxford University Press, New York, 2013), Vol. 33.
[21] James D Bjorken, How black is a constituent quark?? Acta Phys. Pol. B **23**, 637 (1992).
[22] Adrien Florio and Dmitri E Kharzeev, Gibbs entropy from entanglement in electric quenches, Phys. Rev. D **104**, 056021 (2021).
[23] Horacio Casini, Marina Huerta, and Robert C. Myers, Towards a derivation of holographic entanglement entropy, J. High Energy Phys. 05 (2011) 036.
[24] E. Brezin and C. Itzykson, Pair production in vacuum by an alternating field, Phys. Rev. D **2**, 1191 (1970).
[25] V. S. Popov, Pair production in a variable external field (quasiclassical approximation), Zh. Eksp. Teor. Fiz. **61**, 1334 (1971).
[26] Sang Pyo Kim and Don N. Page, Schwinger pair production via instantons in a strong electric field, Phys. Rev. D **65**, 105002 (2002).
[27] Gerald V. Dunne and Christian Schubert, Worldline instantons and pair production in inhomogeneous fields, Phys. Rev. D **72**, 105004 (2005).
[28] Dmitri Kharzeev and Kirill Tuchin, From color glass condensate to quark–gluon plasma through the event horizon, Nucl. Phys. **A753**, 316 (2005).
[29] Holger Gies and Klaus Klingmuller, Pair production in inhomogeneous fields, Phys. Rev. D **72**, 065001 (2005).
[30] Holger Gies and Greger Torgrimsson, Critical Schwinger pair production, Phys. Rev. Lett. **116**, 090406 (2016).
[31] Holger Gies and Greger Torgrimsson, Critical Schwinger pair production II—Universality in the deeply critical regime, Phys. Rev. D **95**, 016001 (2017).
[32] Andrei Mikhailov, Nonlinear waves in AdS/CFT correspondence, arXiv:hep-th/0305196.
[33] Edward Shuryak, Sang-Jin Sin, and Ismail Zahed, A gravity dual of RHIC collisions, J. Korean Phys. Soc. **50**, 384 (2007).
[34] Keun-Young Kim, Sang-Jin Sin, and Ismail Zahed, Diffusion in an expanding plasma using AdS/CFT, J. High Energy Phys. 04 (2008) 047.
[35] Sebastian Grieninger and Ismail Zahed, Out-of-equilibrium photon production and electric conductivity in a holographic Bjorken expanding plasma, Phys. Rev. D **107**, 046017 (2023).